

# Supplemental Information

Max Bertolero<sup>1</sup>, Danielle S. Bassett<sup>2</sup>, and Azeez Adebimpe<sup>3</sup>

<sup>1</sup>University of California, Berkeley

<sup>2</sup>Affiliation not available

<sup>3</sup>University of Pennsylvania

September 14, 2018

## Materials and Methods

### Brain network construction

Generally, to perform network analyses one must define the two important elements of the network – nodes and edges. These two elements are the building blocks of networks and their accurate definitions are very important for any network models (Butts 2009). The standard method of defining network nodes in the field of network neuroscience is to consider neuroimaging data such fMRI and apply a structural atlas or parcellation that separates the whole brain volume into different regions defined by known anatomical differences. Network nodes thus represent the collection of voxels within anatomically defined region. The network edges reflect statistical dependencies between the activity time series of two nodes. In this study, the brain is parcellated into 112 subcortical and cortical regions (see Supplementary Table 1) defined by the structural Harvard-Oxford atlas of the fMRIB (Smith et al. 2004; Woolrich et al. 2009). Each region’s activity is given by the mean time series across all voxels within that region.

The edge weights that link network nodes (brain regions) were defined as the wavelet transform coherence (WTC) (Torrence and Compo 1998), smoothed over time and frequency to avoid bias toward unity coherence. We use Morlet wavelets with coefficients given by:

$$w(t, f) = (\sigma_t \sqrt{\pi})^{-\frac{1}{2}} e^{-i2\pi ft} e^{-\frac{t^2}{2\sigma_t^2}}$$

, where  $f$  is the centre frequency and  $\sigma_t$  is the temporal standard deviation. The time-frequency estimate,  $X(t, f)$  of time series  $x(t)$  was computed by a convolution with the wavelet coefficients:

$$X(t, f) = x(t) * w(t, f).$$

We selected the central frequency of 1/12 Hz corresponding to a spectral width of 0.05 to 0.11 Hz for full width at half maximum. Then the wavelet transform coherence between two time series  $x(t)$  and  $y(t)$  is defined as follows (Torrence and Compo 1998; Cazelles et al. 2007; Grinsted, Moore, and Jevrejeva 2004):

$$TC^2(f, t) = \frac{|S(s^{-1}X_{xy}(t, f))|^2}{S(s^{-1}|X_x(t, f)|^2) \cdot S(s^{-1}|X_y(t, f)|^2)}$$

where  $X_{xy}$  is the cross-wavelet of  $X_x$  and  $X_y$ ,  $s$  is the scale which depends on the frequency (Cazelles et al. 2007; Grinsted, Moore, and Jevrejeva 2004), and  $S$  is the smoothing operator. This definition closely resembles that of a traditional coherence, with the marked difference that the wavelet coherence provides a localized correlation coefficient in both time and frequency. Higher scales are required for lower frequency signals (Cazelles et al. 2007; Grinsted, Moore, and Jevrejeva 2004) and in this study, we used  $s=32$  for the

smoothing operation. This procedure was repeated for all pair of regions yielding the 112 by 112 adjacency matrix,  $\mathbf{A}$ , representing the functional connectivity between brain regions.

## Network modularity

In neuroscience, the term network modularity can be used to refer to the concept that brain regions cluster into modules or *communities*. These communities can be identified computationally using machine learning techniques in the form of community detection algorithms (Girvan and Newman 2001). A community of nodes is a group of nodes that are tightly interconnected. In this study, we implemented a generalized Louvain community detection algorithm (De Meo et al. 2011; Mucha et al. 2010) which considers multiple adjacency matrices as slices of a multilayer network, and which then produces a partition of brain regions into modules that reflects each subject’s community structure across the multiple stages of learning instantiated in the four days of task practice. The multilayer network was constructed by connecting the adjacency matrices of all scans and subjects with interlayer links. We then maximized a multilayer modularity quality function,  $Q$ , that seeks a partition of nodes into communities that maximizes intra-community connections (Mucha et al. 2010):

$$Q = \frac{1}{2\mu} \sum_{ijs} [(A_{ijs} - \gamma_s V_{ijs})\delta_{sr} + \delta_{ij}\omega_{jrs}] \delta(g_{is}, g_{jr}),$$

where  $A_{ijs}$  is the  $ij^{\text{th}}$  element of the adjacency matrix of slice  $s$ , and element  $V_{ijs}$  is the component of the null model matrix tuned by the structural resolution parameter  $\gamma$ . In this study, we set  $\gamma=1$ , which is the standard practice in the field when no *a priori* hypotheses exist to otherwise inform the choice of  $\gamma$ . We employed the Newman-Girvan null model within each layer by using  $V_{ijs} = \frac{k_{is}k_{js}}{2m_s}$ , where  $k$  is the total edge weight and  $m_s$  is the total edge weight in slice  $s$ . The interslice coupling parameter,  $\omega_{jrs}$ , is the connection strength of the interlayer link between node  $j$  in slice  $s$  and node  $j$  in slice  $r$ , and the total edge in the network is  $\mu = \frac{1}{2} \sum_{jrs} \kappa_{jrs}$ . The node strength,  $\kappa_{jrs}$ , is the sum of the intraslice strength and interslice strength:  $\kappa_{jrs} = k_{jrs} + c_{jrs}$ , and  $c_{jrs} = \sum_s \omega_{jrs}$ . In this study, we set  $\omega = 1$ , which is the standard practice in the field when no *a priori* hypotheses exist to otherwise inform the choice of  $\omega$ . Finally, the indicator  $\delta(g_i, g_j) = 1$  if nodes  $i$  and  $j$  are assigned to the same community, and is 0 otherwise. We obtained a partition of the brain into communities for each scan and subject, and from that ensemble of partitions we constructed a module allegiance matrix (Bassett et al., 2015), whose elements correspond to the probability that two regions belong to the same community across all scans and subjects. The seven network communities generated with this procedure are shown in Table 1 in the main text.

## Edge strength

In complementary analyses, we also investigated which regions of the brain were characterized by high strength within the network. The edge strength of node  $i$  is defined as

$$S_i = \frac{1}{N-1} \sum_{j \in N} a_{ij}$$

,

where  $a_{ij}$  is the  $ij^{\text{th}}$  element of the adjacency matrix with  $N$  nodes.

## Supplementary results

### ISC and ISFC

Across subjects, the ISC of many brain regions was consistent from day to day during the value learning task. In particular, the fusiform, lingual gyrus, several areas in the occipital lobe, and precentral regions’ activity were most consistently correlated across the subjects (Fig. S1A). The correlation strength was lower

on day four but the lingual, fusiform gyrus and lateral occipital lobe were still found to be significantly correlated across the subjects. In general, the ISFC was lower on day one but increased in day two (Fig. 2 in the main text and Fig. S1B); specifically, ISFC was high in the right precuneus and superior temporal pole, regions of the default mode network, and regions of the primary visual system. Other regions with significantly high ISFC included the left middle temporal gyrus, hippocampus, and medial prefrontal cortex. On day four, ISFC was significantly high across the subjects in regions that include superior and middle frontal gyri, superior parietal, angular gyrus, posterior cingulate gyrus, precuneus and cuneus, supercalcarine cortex, lateral occipital cortex, occipital fusiform gyrus, lingual gyrus, hippocampus, and insular cortex.

As a null model, we also computed the ISC for the rest condition, during which fMRI data was also acquired in each of the four days of the experiment (Fig. S2A-S2B). We observed that the average ISC was much lower during the rest condition compared to during the value learning task; in fact, the average ISC was statistically indistinguishable from zero. This observation is perhaps not so surprising when one considers that during the rest condition, activity is no longer time locked to any stimulus, and therefore subject’s brain dynamics are allowed to evolve independently. Moreover, we observed that the ISC was similar across all four days of the resting condition, not varying appreciably across days; the temporal consistency of the resting ISC was also upheld in all network communities (Fig. S2A-S2B). Similarly, we observed that the ISFC was similar across all four days of the resting condition, not varying appreciably across days; the temporal consistency of the resting ISFC was also upheld in all network communities (Fig. S2C-S2D). Thus, our results regarding the temporal evolution of ISC and ISFC are driven by learning, not time, as they are only observed during the learning condition, and not during the resting condition.

## Functional integration

As shown in Figure 3 in the main manuscript, the community detection procedure yielded seven communities defined by the functional activity and structural location of network modules. The seven communities (see Table 1 in the main text) are fronto-temporal (FT), sensorimotor (SM), default mode network (DMN), auditory (AUD), language (LAN), visual (VIS), and the three regions putamen, caudate, and thalamus (PCT). The functional connectivity pattern during the task shows consistent functional connectivity patterns across all four days of the experiment (Fig. S3). There were strong functional connections within each system, and most especially in the VIS, DMN and SM modules. The pattern of functional connectivity was consistent across days, and we observed strong functional connections between the DMN, sensorimotor, and visual networks, suggesting that these regions are more integrated than other networks during value learning.

## References

Brain regions present in the Harvard-Oxford cortical and subcortical atlas as provided by FSL.

---

Frontal pole	Cingulate gyrus, anterior
Insular cortex	Cingulate gyrus, posterior
Superior frontal gyrus	Precuneus cortex
Middle frontal gyrus	Cuneus cortex
Inferior frontal gyrus, pars triangularis	Orbital frontal cortex
Inferior frontal gyrus, pars opercularis	Parahippocampal gyrus, anterior
Precentral gyrus	Parahippocampal gyrus, posterior
Temporal pole	Lingual gyrus
Superior temporal gyrus, anterior	Temporal fusiform cortex, anterior
Superior temporal gyrus, posterior	Temporal fusiform cortex, posterior
Middle temporal gyrus, anterior	Temporal occipital fusiform cortex
Middle temporal gyrus, posterior	Occipital fusiform gyrus

Middle temporal gyrus, temporooccipital	Fronal operculum cortex
Inferior temporal gyrus, anterior	Central opercular cortex
Inferior temporal gyrus, posterior	Parietal operculum cortex
Inferior temporal gyrus, temporooccipital	Planum polare
Postcentral gyrus	Heschl's gyrus
Superior parietal lobule	Planum temporale
Supramarginal gyrus, anterior	Supercalcarine cortex
Supramarginal gyrus, posterior	Occipital pole
Angular gyrus	Caudate
Lateral occipital cortex, superior	Putamen
Lateral occipital cortex, inferior	Globus pallidus
Intracalcarine cortex	Thalamus
Frontal medial cortex	Nucleus Accumbens
Supplemental motor area	Amygdala
Subcallosal cortex	Hippocampus
Paracingulate gyrus	Brainstem

---

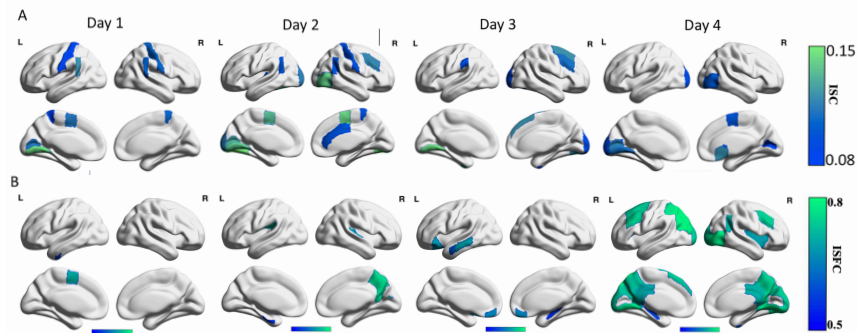


Figure 1: **ISC and ISFC maps during the task condition.** (A) The ISC was significant ( $p < 0.05$ , corrected for multiple comparisons) in the lingual gyrus and sensorimotor regions across all four days of task practice. Other regions that showed significant ISC across only the first three days of task practice include the supramarginal gyrus, and across only the last three days of task practice include the lateral occipital lobe. (B) The ISFC was lower in day 1 but increased steadily with higher ISFC strength in day 3 and day 4. Regions with significant ISFC ( $p < 0.05$ , corrected for multiple comparisons) included sensorimotor areas, lingual gyrus, supramarginal gyrus, anterior cingulate gyrus and frontal pole, particularly in the third and fourth day of task practice.

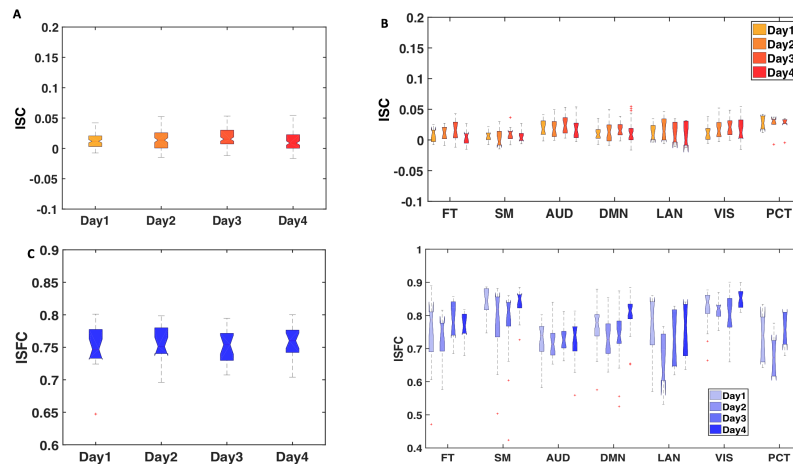


Figure 2: **ISC and ISFC during the resting state condition.** (A) The average ISC during the resting state condition is similar across all four days of the experiment, (B) with no clear differences across each network community. (C) The ISFC was lower on day 2 of the experiment, and (D) the same patterns were observed for all network communities. The fronto-temporal (FT) and auditory (AUD) networks had lower ISFC compared to other networks.

## References

- Butts, Carter T. 2009. “Revisiting the Foundations of Network Analysis”. *Science* 325 (5939). American Association for the Advancement of Science: 414–16.
- Smith, Stephen M, Mark Jenkinson, Mark W Woolrich, Christian F Beckmann, Timothy EJ Behrens, Heidi Johansen-Berg, Peter R Bannister, et al. 2004. “Advances in Functional and Structural MR Image Analysis and Implementation as FSL”. *Neuroimage* 23. Elsevier: S208–S219.
- Woolrich, Mark W, Saad Jbabdi, Brian Patenaude, Michael Chappell, Salima Makni, Timothy Behrens, Christian Beckmann, Mark Jenkinson, and Stephen M Smith. 2009. “Bayesian Analysis of Neuroimaging Data in FSL”. *Neuroimage* 45 (1). Elsevier: S173–S186.
- Torrence, Christopher, and Gilbert P Compo. 1998. “A Practical Guide to Wavelet Analysis”. *Bulletin of the American Meteorological Society* 79 (1): 61–78.
- Cazelles, Bernard, Mario Chavez, Guillaume Constantin de Magny, Jean-Francois Guégan, and Simon Hales. 2007. “Time-Dependent Spectral Analysis of Epidemiological Time-Series with Wavelets”. *Journal of the Royal Society Interface* 4 (15). The Royal Society: 625–36.
- Grinsted, Aslak, John C Moore, and Svetlana Jevrejeva. 2004. “Application of the Cross Wavelet Transform and Wavelet Coherence to Geophysical Time Series”. *Nonlinear Processes in Geophysics* 11 (5/6): 561–66.
- Girvan, Michelle, and Mark EJ Newman. 2001. “Community Structure in Social and Biological Networks”. *Proc. Natl. Acad. Sci. USA* 99 (cond-mat/0112110): 8271–76.

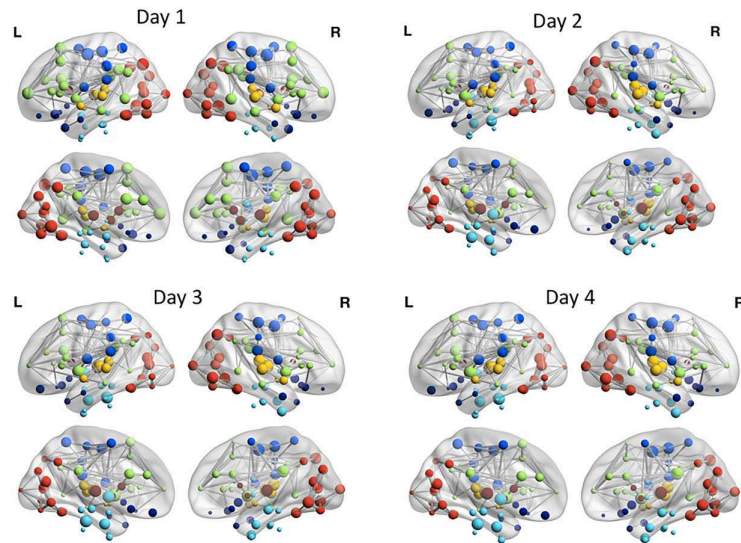


Figure 3: **Functional connectivity pattern during value learning.** Across the days, the functional connectivity is relatively strong within DMN, sensorimotor, and visual networks across all four days of task practice. We also observe interconnectivity between networks, indicating network integration during value learning. Edges shown are those whose functional connectivity strength has a statistical significance of  $p=0.05$  or less.

De Meo, Pasquale, Emilio Ferrara, Giacomo Fiumara, and Alessandro Provetti. 2011. “Generalized Louvain Method for Community Detection in Large Networks”. In *Intelligent Systems Design and Applications (ISDA), 2011 11th International Conference On* , 88–93. IEEE.

Mucha, Peter J, Thomas Richardson, Kevin Macon, Mason A Porter, and Jukka-Pekka Onnela. 2010. “Community Structure in Time-Dependent, Multiscale, and Multiplex Networks”. *Science* 328 (5980). American Association for the Advancement of Science: 876–78.

Bassett, Danielle S, Nicholas F Wymbs, Mason A Porter, Peter J Mucha, Jean M Carlson, and Scott T Grafton. 2011. “Dynamic Reconfiguration of Human Brain Networks during Learning”. *Proceedings of the National Academy of Sciences* 108 (18). National Acad Sciences: 7641–46.

Nicosia, Vincenzo, John Tang, Cecilia Mascolo, Mirco Musolesi, Giovanni Russo, and Vito Latora. 2013. “Graph Metrics for Temporal Networks”. In *Temporal Networks* , 15–40. Springer.

## References

Danielle S Bassett, Muzhi Yang, Nicholas F Wymbs, and Scott T Grafton. Learning-induced autonomy of sensorimotor systems. *Nature Neuroscience*, 18(5):744–751, apr 2015. doi: 10.1038/nn.3993. URL <https://doi.org/10.1038%2Fnn.3993>.